

# Real-Time Implementation of a LQR-Based Controller for the Stabilization of a Double Inverted Pendulum

Amanda Bernstein and Hien Tran, *Member, SIAM*

**Abstract**—The problem of real-time implementation of a linear quadratic regulator (LQR)-based controller for the balance of a double inverted pendulum (DIP) mounted on a cart is presented. Physically, the DIP system is stabilized when the two pendulums are aligned in a vertical position. The mathematical model for the dynamics of a DIP can be derived using the Lagrange’s energy method, which is computed from the calculation of the total potential and kinetic energies of the system. This results in a highly nonlinear system of three second-order ordinary differential equations. The nonlinear system is linearized around its zero equilibrium state and LQR controller is implemented in real-time to stabilize the DIP system (i.e., to keep DIP in an upright position). Both simulation and real-time experimental results are presented.

**Index Terms**—double inverted pendulum, LQR, feedback controller, real-time implementation.

## I. INTRODUCTION

THE double inverted pendulum (DIP) system is an extension of the single inverted pendulum (with one additional pendulum added to the single inverted pendulum), mounted on a moving cart. The DIP system is a standard model of multivariable, nonlinear, unstable system, which can be used for pedagogy as well as for the introduction of intermediate and advanced control concepts. There are two types of control synthesis for an inverted pendulum, swing-up and stabilization. One of the most popular control methods for swinging up the inverted pendulum is based on the energy method (see [1] and the references therein). The stabilization problem of an inverted pendulum is a classical control example for testing of linear and nonlinear controllers (see, e.g., [1], [2], [3]). Several control design approaches have been applied for the stabilization of the double inverted pendulum including the linear quadratic regulator [4], the state-dependent Riccati equation, optimal neural network [5], and model predictive control [3]. To our knowledge, these studies only use numerical simulations to

Manuscript received December 12, 2016.

A. Bernstein is a graduate student with the Department of Mathematics, North Carolina State University, Raleigh, NC 27695 USA e-mail: ascoons@ncsu.edu.

H. Tran is with the Department of Mathematics, North Carolina State University, Raleigh, NC 27695 USA e-mail: tran@ncsu.edu.

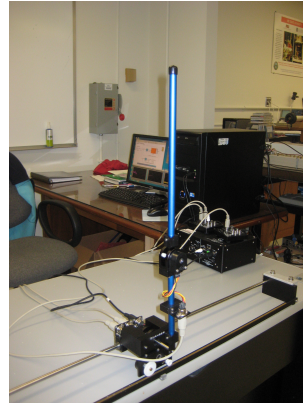


Fig. 1: Double inverted pendulum mounted on a Quanser linear servo base unit (IP02).

test the feasibility of the control methodologies and do not provide real-time experimental implementation on a physical system.

In this paper, we present the real-time implementation of a LQR-based feedback control for the stabilization about the upright position of the double inverted pendulum mounted on a cart. The apparatus of the DIP system, which was provided by Quanser Consulting Inc. (119 Spy Court, Markham, Ontario, L3R 5H6, Canada), is depicted in Fig. 1. The DIP system consists of two aluminum rods; one seven inches long and the other 12 inches long. The aluminums are mounted on the linear servo base unit (IP02) consisting of a cart driven by a DC motor and two encoders. One encoder is used to measure the cart’s position while the other encoder is used to sense the short link angle. The longer link angle is measured by an encoder mounted on the pendulum itself. Based on these measurements of the cart position and the two pendulum angles, a voltage is computed using the LQR control theory to move the cart back and forth to balance the two pendulums in the upright, vertical position.

## II. DIP SYSTEM MODEL

### A. Frame of Reference

Figure 2 shows a free body diagram of the DIP system mounted on a cart. The system consists of

two rods connected to each other by a hinge with the lower rod connected to the motorized cart. The corresponding nomenclature for this system is given in Appendix A. The angle  $\alpha$  of the lower rod is zero when the rod is pointed perfectly upwards, and the angle  $\theta$  of the upper rod is zero when it is perfectly in line with the lower rod. It should be noted that, in the literature, the models for the DIP system are derived with the angle  $\theta$  measured with respect to the vertical axis [5] (instead of relative to the lower pendulum rod as in this paper). We define the positive sense of the rotation to be counterclockwise and the displacement to be towards the right when facing the cart.

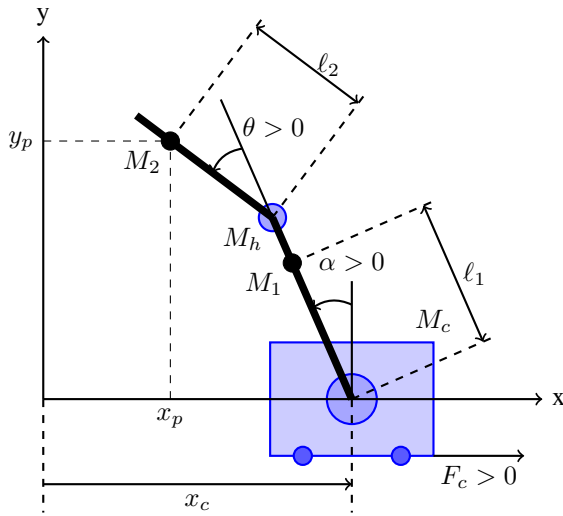


Fig. 2: Free body diagram of the DIP mounted on a cart.

### B. Equations of Motion

We use Lagrange's energy method to derive the equations of motion for the DIP system. The single input is the driving force  $F_c$  generated by the DC motor and acting on the cart via the motor pinion. The Lagrangian of the motion is computed from the calculation of the total potential and kinetic energies of the system.

In order to calculate the energy of the system, we first determine the absolute cartesian coordinates for the center of gravity of each pendulum rod and the hinge. For the lower rod, pendulum 1, the center of gravity is located at

$$\begin{aligned} x_1(t) &= x_c(t) - \ell_1 \sin(\alpha(t)) \\ y_1(t) &= \ell_1 \cos(\alpha(t)) \end{aligned} \quad (1)$$

and for the upper rod, pendulum 2, the center of gravity is located at

$$\begin{aligned} x_2(t) &= x_c(t) - \ell_2 \sin(\alpha(t) + \theta(t)) \\ &\quad - L_1 \sin(\alpha(t)) \\ y_2(t) &= \ell_2 \cos(\alpha(t) + \theta(t)) + L_1 \cos(\alpha(t)). \end{aligned} \quad (2)$$

The center of gravity of the hinge is located at

$$\begin{aligned} x_h(t) &= x_c(t) - L_1 \sin(\alpha(t)) \\ y_h(t) &= L_1 \cos(\alpha(t)). \end{aligned} \quad (3)$$

We determine the linear velocity of each component by taking derivatives with respect to time of (1), (2), and (3) to obtain

$$\begin{aligned} x'_1(t) &= x'_c(t) - \ell_1 \alpha'(t) \cos(\alpha(t)) \\ y'_1(t) &= -\ell_1 \alpha'(t) \sin(\alpha(t)) \\ x'_2(t) &= x'_c(t) - \ell_2 (\alpha'(t) + \theta'(t)) \cos(\alpha(t) \\ &\quad + \theta(t)) - L_1 \alpha'(t) \cos(\alpha(t)) \\ y'_2(t) &= -\ell_2 (\alpha'(t) + \theta'(t)) \sin(\alpha(t) + \theta(t)) \\ &\quad - L_1 \alpha'(t) \sin(\alpha(t)) \\ x'_h(t) &= x'_c(t) - L_1 \alpha'(t) \cos(\alpha(t)) \\ y'_h(t) &= -L_1 \alpha'(t) \sin(\alpha(t)). \end{aligned} \quad (4)$$

1) *Potential Energy*: The total potential energy in a system,  $V_T$ , is the energy a system has due to work being or having been done to it. Typically potential energy is due to either vertical displacement (gravitational potential energy) or spring-related displacement (elastic potential energy). Here, there is no elastic potential energy, just the potential energy due to gravity. However, since the cart is limited to horizontal motion, it has no gravitational potential energy. The potential energies of the pendulum rods and the hinge are given by

$$V_1(t) = M_1 g y_1 = M_1 g \ell_1 \cos(\alpha(t)) \quad (5)$$

$$\begin{aligned} V_2(t) &= M_2 g y_2 = M_2 g [\ell_2 \cos(\alpha(t) + \theta(t)) \\ &\quad + L_1 \cos(\alpha(t))] \end{aligned} \quad (6)$$

$$V_h(t) = M_h g y_h = M_h g L_1 \cos(\alpha(t)). \quad (7)$$

Then the total potential energy of the system is the sum of each component's potential energy. Summing (5), (6), and (7) and rearranging, we obtain

$$\begin{aligned} V_T(t) &= [M_1 g \ell_1 + M_2 g L_1 + M_h g L_1] \cos(\alpha(t)) \\ &\quad + M_2 g \ell_2 \cos(\alpha(t) + \theta(t)). \end{aligned} \quad (8)$$

2) *Kinetic Energy*: The total kinetic energy of a system,  $T_T$ , is the amount of energy due to motion. For the DIP system, the kinetic energy is the sum of the translational and rotational energies of each component.

First, we consider the cart which has kinetic energy due to its linear motion along the track and due to the rotation of the DC motor. The translational kinetic energy of the cart is given by

$$T_{ct}(t) = \frac{1}{2} M_c (x'_c(t))^2. \quad (9)$$

The rotational kinetic energy of the cart's DC motor is given by

$$T_{cr}(t) = \frac{1}{2} J_m (\omega_c(t))^2, \quad (10)$$

where

$$\omega_c(t) = \frac{K_g}{r_{mp}} x'_c(t). \quad (11)$$

Then the total kinetic energy of the cart is the sum of translational and rotational kinetic energies,

$$T_c(t) = \frac{1}{2} \left[ M_c + \frac{J_m K_g^2}{r_{mp}^2} \right] (x'_c(t))^2. \quad (12)$$

Next we consider the kinetic energy of each pendulum rod. For each, we assume the mass of the pendulum is concentrated at its center of gravity. Then, the translational kinetic energy of the lower pendulum rod is given by

$$\begin{aligned} T_{1t}(t) &= \frac{1}{2} M_1 [(x'_1(t))^2 + (y'_1(t))^2] \\ &= \frac{1}{2} M_1 [(x'_c(t))^2 \\ &\quad - 2\ell_1 x'_c(t) \alpha'(t) \cos(\alpha(t)) + \ell_1^2 (\alpha'(t))^2], \end{aligned} \quad (13)$$

and the rotational kinetic energy is given by

$$T_{1r}(t) = \frac{1}{2} I_1 (\alpha'(t))^2. \quad (14)$$

Thus, the total kinetic energy for the lower pendulum rod is given by

$$\begin{aligned} T_1(t) &= \frac{1}{2} M_1 [(x'_c(t))^2 - 2\ell_1 x'_c(t) \alpha'(t) \cos(\alpha(t)) \\ &\quad + \ell_1^2 (\alpha'(t))^2] + \frac{1}{2} I_1 (\alpha'(t))^2. \end{aligned} \quad (15)$$

Similarly, the translational and rotational kinetic energies of the upper pendulum rod are given by

$$\begin{aligned} T_{2t}(t) &= \frac{1}{2} M_2 [(x'_2(t))^2 + (y'_2(t))^2] \\ &= \frac{1}{2} M_2 [(x'_c(t))^2 - 2\ell_2 x'_c(t) (\alpha'(t) + \theta'(t)) \\ &\quad \times \cos(\alpha(t) + \theta(t)) - 2L_1 x'_c(t) \alpha'(t) \cos(\alpha) \\ &\quad + 2L_1 \ell_2 \alpha'(t) (\alpha'(t) + \theta'(t)) \cos(2\alpha + \theta) \\ &\quad + \ell_2^2 (\alpha'(t) + \theta'(t))^2 + L_1^2 (\alpha'(t))^2] \end{aligned}$$

$$T_{2r}(t) = \frac{1}{2} I_2 (\theta'(t))^2$$

for a total kinetic energy of

$$\begin{aligned} T_2(t) &= \frac{1}{2} M_2 [(x'_c(t))^2 - 2\ell_2 x'_c(t) (\alpha'(t) + \theta'(t)) \\ &\quad \times \cos(\alpha(t) + \theta(t)) - 2L_1 x'_c(t) \alpha'(t) \cos(\alpha) \\ &\quad + 2L_1 \ell_2 \alpha'(t) (\alpha'(t) + \theta'(t)) \cos(2\alpha + \theta) \\ &\quad + \ell_2^2 (\alpha'(t) + \theta'(t))^2 + L_1^2 (\alpha'(t))^2] \\ &\quad + \frac{1}{2} I_2 (\theta'(t))^2. \end{aligned} \quad (16)$$

Finally, the hinge has only translational kinetic energy since it cannot rotate about its own axis.

Therefore the total kinetic energy of the hinge is given by

$$\begin{aligned} T_h(t) &= \frac{1}{2} M_h [(x'_h(t))^2 + (y'_h(t))^2] \\ &= \frac{1}{2} M_h [(x'_c(t))^2 - 2L_1 x'_c(t) \alpha'(t) \cos(\alpha(t)) \\ &\quad + L_1^2 (\alpha'(t))^2]. \end{aligned} \quad (17)$$

Summing (12), (15), (16), and (17) we obtain the total kinetic energy of the system

$$\begin{aligned} T_T(t) &= \frac{1}{2} \left[ M_c + \frac{J_m K_g^2}{r_{mp}^2} + M_1 + M_2 + M_h \right] (x'_c(t))^2 \\ &\quad - [M_1 \ell_1 + M_2 L_1 + M_h L_1] x'_c(t) \alpha'(t) \cos(\alpha(t)) \\ &\quad + \frac{1}{2} [M_1 \ell_1^2 + I_1 + M_2 L_1^2 + M_h L_1^2] (\alpha'(t))^2 \\ &\quad - M_2 \ell_2 x'_c(t) (\alpha'(t) + \theta'(t)) \cos(\alpha(t) + \theta(t)) \\ &\quad + M_2 L_1 \ell_2 \alpha'(t) (\alpha'(t) + \theta'(t)) \cos(2\alpha(t) + \theta(t)) \\ &\quad + \frac{1}{2} M_2 \ell_2^2 (\alpha'(t) + \theta'(t))^2 + \frac{1}{2} I_2 (\theta'(t))^2. \end{aligned} \quad (18)$$

3) *Lagrange's Equations:* The Lagrangian,  $\mathcal{L}$ , of a system is given by the difference between the total kinetic and potential energies

$$\mathcal{L}(t) = T_T(t) - V_T(t). \quad (19)$$

Substituting (8) and (18) into (19) we obtain

$$\begin{aligned} \mathcal{L}(t) &= \frac{1}{2} \left[ M_c + \frac{J_m K_g^2}{r_{mp}^2} + M_1 + M_2 + M_h \right] (x'_c(t))^2 \\ &\quad - [M_1 \ell_1 + M_2 L_1 + M_h L_1] x'_c(t) \alpha'(t) \cos(\alpha(t)) \\ &\quad + \frac{1}{2} [M_1 \ell_1^2 + I_1 + M_2 L_1^2 + M_h L_1^2] (\alpha'(t))^2 \\ &\quad - M_2 \ell_2 x'_c(t) (\alpha'(t) + \theta'(t)) \cos(\alpha(t) + \theta(t)) \\ &\quad + M_2 L_1 \ell_2 \alpha'(t) (\alpha'(t) + \theta'(t)) \cos(2\alpha(t) + \theta(t)) \\ &\quad + \frac{1}{2} M_2 \ell_2^2 (\alpha'(t) + \theta'(t))^2 + \frac{1}{2} I_2 (\theta'(t))^2 \\ &\quad - g [M_1 \ell_1 + M_2 L_1 + M_h L_1] \cos(\alpha(t)) \\ &\quad - M_2 g \ell_2 \cos(\alpha(t) + \theta(t)). \end{aligned} \quad (20)$$

By definition, Lagrange's equations are given by

$$\frac{\partial}{\partial t} \left( \frac{\partial}{\partial x'_c} \mathcal{L} \right) - \frac{\partial}{\partial x_c} \mathcal{L} = Q_1 \quad (21)$$

$$\frac{\partial}{\partial t} \left( \frac{\partial}{\partial \alpha'} \mathcal{L} \right) - \frac{\partial}{\partial \alpha} \mathcal{L} = Q_2 \quad (22)$$

$$\frac{\partial}{\partial t} \left( \frac{\partial}{\partial \theta'} \mathcal{L} \right) - \frac{\partial}{\partial \theta} \mathcal{L} = Q_3, \quad (23)$$

where  $Q_1$ ,  $Q_2$ , and  $Q_3$  are the generalized forces applied to each of the generalized coordinates. When we compute the generalized forces we neglect the nonlinear Coulomb friction and the force due to the

pendulum's action on the linear cart. Therefore the generalized forces are

$$Q_1(t) = F_c(t) - B_c x'_c(t) \quad (24)$$

$$Q_2(t) = -B_1 \alpha'(t) \quad (25)$$

$$Q_3(t) = -B_2 \theta'(t). \quad (26)$$

We substitute (24), (25), and (26) into (21), (22), and (23), respectively, to obtain

$$\frac{\partial}{\partial t} \left( \frac{\partial \mathcal{L}}{\partial x'_c} \right) - \frac{\partial \mathcal{L}}{\partial x_c} = F_c(t) - B_c x'_c(t) \quad (27)$$

$$\frac{\partial}{\partial t} \left( \frac{\partial \mathcal{L}}{\partial \alpha'} \right) - \frac{\partial \mathcal{L}}{\partial \alpha} = -B_1 \alpha'(t) \quad (28)$$

$$\frac{\partial}{\partial t} \left( \frac{\partial \mathcal{L}}{\partial \theta'} \right) - \frac{\partial \mathcal{L}}{\partial \theta} = -B_2 \theta'(t). \quad (29)$$

Using (20), we take the derivatives indicated in (21) and rearrange to obtain

$$\begin{aligned} & \left[ M_c + \frac{J_m K_g^2}{r_{mp}^2} + M_1 + M_2 + M_h \right] x''_c(t) \\ & - \left[ (M_1 \ell_1 + M_2 L_1 + M_h L_1) \cos(\alpha(t)) \right. \\ & \quad \left. + M_2 \ell_2 \cos(\alpha(t) + \theta(t)) \right] \alpha''(t) \\ & - M_2 \ell_2 \cos(\alpha(t) + \theta(t)) \theta''(t) + B_c x'_c(t) \\ & \left[ \left[ (M_1 \ell_1 + M_2 L_1 + M_h L_1) \sin(\alpha(t)) \right. \right. \\ & \quad \left. \left. + M_2 \ell_2 \sin(\alpha(t) + \theta(t)) \right] \alpha'(t) + \right. \\ & \quad \left. 2M_2 \ell_2 \sin(\alpha(t) + \theta(t)) \theta'(t) \right] \alpha'(t) \\ & + M_2 \ell_2 \sin(\alpha(t) + \theta(t)) (\theta'(t))^2 = F_c(t). \end{aligned} \quad (30)$$

Similarly, taking the derivatives indicated in (22) of (20) and rearranging yields

$$\begin{aligned} & - \left[ (M_1 \ell_1 + M_2 L_1 + M_h L_1) \cos(\alpha(t)) \right. \\ & \quad \left. + M_2 \ell_2 \cos(\alpha(t) + \theta(t)) \right] x''_c(t) \\ & + \left[ M_1 \ell_1^2 + I_1 + M_2 L_1^2 + M_h L_1^2 + M_2 \ell_2^2 \right. \\ & \quad \left. + 2M_2 L_1 \ell_2 \cos(2\alpha(t) + \theta(t)) \right] \alpha''(t) \\ & + \left[ M_2 L_1 \ell_2 \cos(2\alpha(t) + \theta(t)) + M_2 \ell_2^2 \right] \theta''(t) \\ & + \left[ B_1 - 2M_2 L_1 \ell_2 \sin(2\alpha(t) \right. \\ & \quad \left. + \theta(t)) (\alpha'(t) + \theta'(t)) \right] \alpha'(t) \\ & - M_2 L_1 \ell_2 \sin(2\alpha(t) + \theta(t)) (\theta'(t))^2 \\ & - g \left[ M_1 \ell_1 + M_2 L_1 + M_h L_1 \right] \sin(\alpha(t)) \\ & - g M_2 \ell_2 \sin(\alpha(t) + \theta(t)) = 0. \end{aligned} \quad (31)$$

Likewise, we take the derivatives indicated in (23) and rearrange to obtain

$$\begin{aligned} & -M_2 \ell_2 \cos(\alpha(t) + \theta(t)) x''_c(t) \\ & + \left[ M_2 L_1 \ell_2 \cos(2\alpha(t) + \theta(t)) + M_2 \ell_2^2 \right] \alpha''(t) \\ & + \left[ M_2 \ell_2^2 + I_2 \right] \theta''(t) \\ & - M_2 L_1 \ell_2 \sin(2\alpha(t) + \theta(t)) (\alpha'(t))^2 + B_2 \theta'(t) \\ & - g M_2 \ell_2 \sin(\alpha(t) + \theta(t)) = 0. \end{aligned} \quad (32)$$

Equations (30), (31), and (32) are the equations of motion for the DIP system. The units and parameter values for all parameters in the model equations are given in Appendix B. Finally, the control input in the equations of motion is the force generated by the motorized cart,  $F_c(t)$  (see (30)), but in our real-time implementation the input to the DIP system is the cart's DC motor voltage,  $V_m(t)$ . Using Kirchhoff's voltage laws and physical properties of our DIP system, we can express  $F_c$  as a function of the applied voltage  $V_m$  as

$$F_c(t) = \frac{K_g K_t (V_m(t) r_{mp} - K_g K_m x'_c(t))}{R_m r_{mp}^2}. \quad (33)$$

### III. REAL-TIME LQR CONTROL IMPLEMENTATION

For our real-time implementation of the LQR-based feedback control for the balance of the DIP system in the upright position, we use apparatus designed and provided by Quanser Consulting Inc. (see Fig. 1). This includes a double inverted pendulum mounted on an IP02 servo plant, a VoltPAQ amplifier, and two Q2-USB DAQ control boards. The detailed technical specifications and experimental set up can be found in [6]. For a linear system with a quadratic cost functional in both the state and the control, the optimal feedback control is a linear state feedback law where the control gains are obtained by solving a differential/algebraic Riccati equation (see e.g. [7]). Since the equations of motion for the DIP system, given by (30), (31), and (32), are nonlinear, we first linearized them around the zero equilibrium state to derive a local, approximate optimal control solution.

#### A. Simulation Results

The stabilized control was first tested in simulation with  $Q = \text{diag}(30, 350, 100, 0, 0, 0)$  and  $R = 0.1$  using Matlab Simulink. Here,  $Q$  and  $R$  are the state and input weighting matrices in the cost functional, respectively. The simulation uses an initial condition where the cart is at rest at a position of 0mm and both the upper and lower pendulum angles are deflected to 1 degree. The simulation requires the cart's position to track a square wave (dashed line in Fig. 3 (a)) with amplitude 12.5 mm and a frequency of 0.05 Hz. The

state responses and corresponding control effort are shown in Figs. 3 and 4. All values of the states and the required control effort stay within the possible ranges for our experimental apparatus.

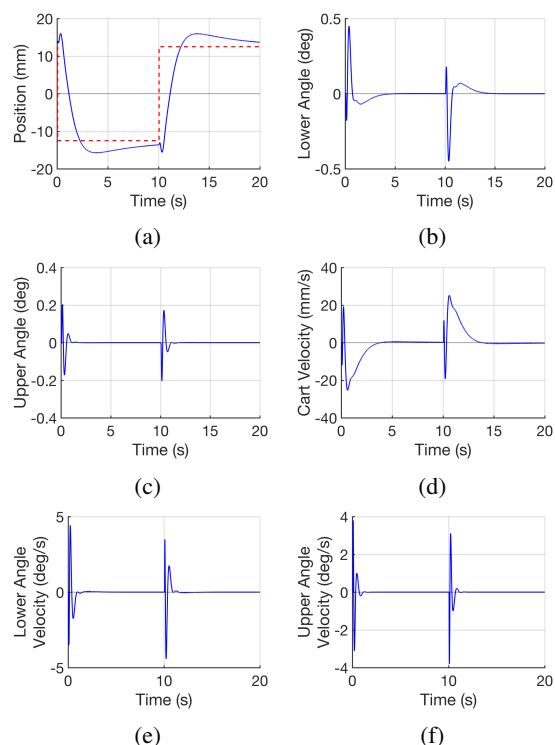


Fig. 3: Simulated state responses: cart position (a) and velocity (d), lower angle position (b) and velocity (e), and upper angle position (c) and velocity (f).

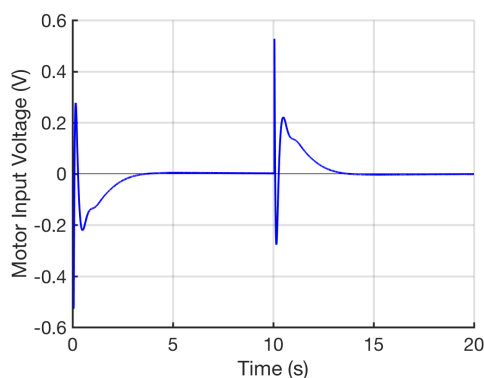


Fig. 4: Simulated control effort.

### B. Experimental Results

The stabilized control was successfully implemented in real time with  $Q = \text{diag}(30, 350, 100, 0, 0, 0)$  and  $R = 0.1$  using Matlab Simulink. The pendulum is manually brought to the upright position and the balancing control automatically takes over. Figs. 5

and 6 show the state responses and corresponding control effort. From the state responses, we can see that the pendulum was successfully balanced in the upright position. The cart does not move more than 40 mm from the center of the track, and the angles never differ from zero by more than 4 degrees. We also note that the controller frequently reaches saturation at -10 V in its effort to keep the pendulum balanced. Future effort will include the design and testing of more robust controllers such as the power series based nonlinear controller discussed in [1], [2].

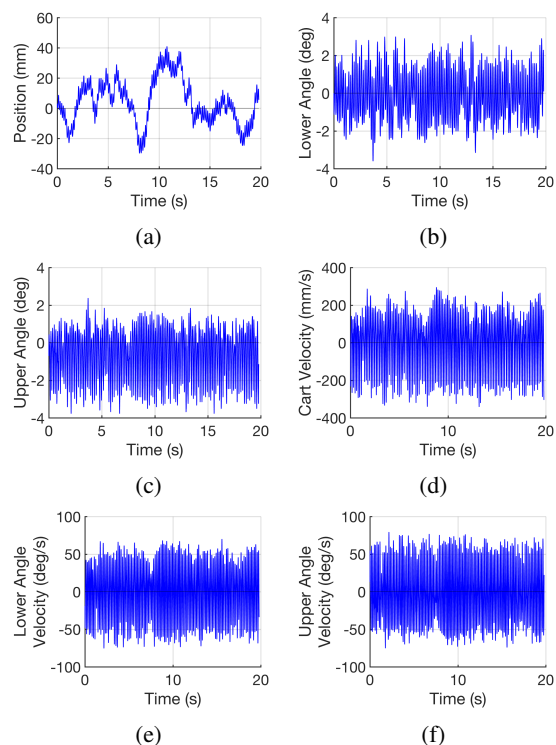


Fig. 5: Experimental state responses: cart position (a) and velocity (d), lower angle position (b) and velocity (e), and upper angle position (c) and velocity (f).

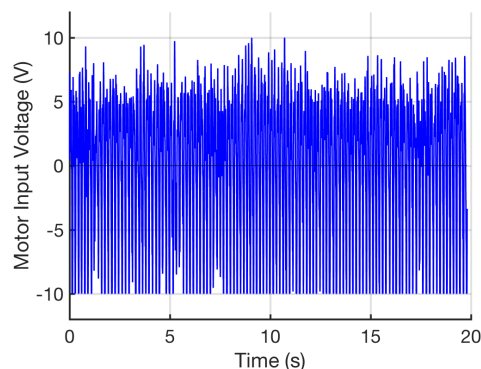


Fig. 6: Experimental control effort.

APPENDIX A  
NOMENCLATURE

	Description
	(Moment of Inertia (MoI), Center of Gravity (CoG))
$\alpha$	Angle of Lower Rod Relative from vertical
$\alpha'$	Lower Pendulum Angular Velocity
$\alpha''$	Lower Pendulum Angular Acceleration
$B_c$	Viscous Damping Coef. (Motor Pinion)
$B_1$	Viscous Damping Coef. (Lower Rod Axis)
$B_2$	Viscous Damping Coef. (Upper Rod Axis)
$F_c$	Cart Driving Force by the DC Motor
$g$	Gravitational Constant
$I_1$	MoI (Lower Rod) at its CoG
$I_2$	MoI (Upper Rod) at its CoG
$J_m$	Rotational MoI of the DC Motor's Output Shaft
$K_g$	Planetary Gearbox Gear Ratio
$\ell_1$	Length of Lower Rod from Pivot to CoG
$\ell_2$	Length of Upper Rod from Hinge to CoG
$L_1$	Total Length of Lower Rod
$\mathcal{L}$	Lagrangian
$M_c$	Cart Mass
$M_h$	Hinge Mass
$M_1$	Lower Rod Mass
$M_2$	Upper Rod Mass
$r_{mp}$	Motor Pinion Radius
$T_{ct}$	Translational Kinetic Energy of the Cart
$T_{cr}$	Rotational Kinetic Energy Due to the Cart's DC Motor
$T_c$	Total Kinetic Energy of the Cart
$T_{1t}$	Translational Kinetic Energy (Lower Rod)
$T_{1r}$	Rotational Kinetic Energy (Lower Rod)
$T_1$	Total Kinetic Energy of the Lower Rod
$T_{2t}$	Translational Kinetic Energy of the Upper Rod
$T_{2r}$	Rotational Kinetic Energy of the Upper Rod
$T_2$	Total Kinetic Energy of the Upper Pendulum
$T_h$	Total Kinetic Energy of the Hinge
$T_T$	Total Kinetic Energy of the System
$V_1$	Potential Energy of the Lower Pendulum
$V_2$	Potential Energy of the Upper Pendulum
$V_h$	Potential Energy of the Hinge
$V_T$	Total Potential Energy of the System
$x_c$	Cart Linear Position
$x'_c$	Cart Velocity
$x''_c$	Cart Acceleration
$x_h$	Absolute x-coord. of the Hinge's CoG
$x_1$	Absolute x-coord. of the Lower Rod's CoG
$x_2$	Absolute x-coord. of the Upper Rod's CoG
$x'_h$	x-comp. of the Velocity of the Hinge's CoG
$x'_1$	x-comp. of the Velocity of the Lower Rod's CoG
$x'_2$	x-comp. of the Velocity of the Upper Rod's CoG
$y_h$	Absolute y-coord. of the Hinge's CoG
$y_1$	Absolute y-coord. of the Lower Rod's CoG
$y_2$	Absolute y-coord. of the Upper Rod's CoG
$y'_h$	y-comp. of the Velocity of the Hinge's CoG
$y'_1$	y-comp. of the Velocity of the Lower Rod's CoG
$y'_2$	y-comp. of the Velocity of the Upper Rod's CoG
$\theta$	Angle of Upper Rod Relative to Lower Rod's Shaft
$\theta'$	Upper Pendulum Angular Velocity
$\theta''$	Upper Pendulum Angular Acceleration
$\omega_c$	Motor Shaft Angular Velocity

APPENDIX B  
MODEL PARAMETER VALUES

	Description	Value
$B_c$	Viscous Damping Coefficient as seen at the Motor Pinion	5.4 N.m.s/rad
$B_1$	Viscous Damping Coefficient as seen at the Lower Rod Axis	0.0024 N.m.s/rad
$B_2$	Viscous Damping Coefficient as seen at the Upper Rod Axis	0.0024 N.m.s/rad
$g$	Gravitational Constant	9.81 m/s <sup>2</sup>
$I_1$	Moment of Inertia of the Lower Rod at its Center of Gravity	2.6347E-4 kg.m <sup>2</sup>
$I_2$	Moment of Inertia of the Upper Rod at its Center of Gravity	1.1987E-3 kg.m <sup>2</sup>
$J_m$	Rotational Moment of Inertia of the DC Motor's Output Shaft	3.9E-7 kg.m <sup>2</sup>
$K_g$	Planetary Gearbox Gear Ratio	3.71
$K_m$	Back-ElectroMotive-Force Const.	0.00767 V.s/rad
$K_t$	Motor Torque Constant	0.00767 N.m/A
$\ell_1$	Length of Lower Pendulum from Pivot to Center of Gravity	0.1143 m
$\ell_2$	Length of Upper Rod from Hinge to Center of Gravity	0.1778 m
$L_1$	Total Length of Lower Rod	0.2096 m
$L_2$	Total Length of Upper Rod	0.3365 m
$M_c$	Cart Mass	0.57 kg
$M_h$	Hinge Mass	0.170 kg
$M_w$	Extra Weight Mass	0.37 kg
$M_1$	Lower Pendulum Mass	0.072 kg
$M_2$	Upper Pendulum Mass	0.127 kg
$R_m$	Motor Armature Resistance	2.6 $\Omega$
$r_{mp}$	Motor Pinion Radius	6.35E-3 m

REFERENCES

- [1] E. Kennedy, *Swing-up and Stabilization of a Single Inverted Pendulum: Real-Time Implementation*. North Carolina State University, 2015.
- [2] E. Kennedy and H. Tran, "Real-time stabilization of a single inverted pendulum using a power series based controller," *Transactions on Engineering Technologies*, pp. 1-14, 2016.
- [3] P. Jaiwat and T. Ohtsuka, "Real-time swing-up of double inverted pendulum by nonlinear model predictive control," in *5th International Symposium on Advanced Control of Industrial Processes, May 28-30, 2014, Hiroshima, JAPAN*, 2014, pp. 290-295.
- [4] S. Yadav, S. Sharma, and N. Singh, "Optimal control of double inverted pendulum using lqr controller," *Int. J. of Advanced Research in Computer Science and Software Engineering*, pp. 189-192, 2012.
- [5] A. Bogdanov, "Optimal control of double inverted pendulum on a cart," in *Technical Report CSE-04-006*, 2004.
- [6] *Linear Motion Servo Plants: IP012 - Double Inverted Pendulum (DBIP) Laboratory Manual*, Quanser Consulting, Inc., Document number:535, Revision:04.
- [7] B. Anderson and J. Moore, *Optimal Control: Linear Quadratic Methods*. Prentice-Hall, 1990.